The application of remote sensing techniques to the study of ophiolites

Article *in* Earth-Science Reviews · August 2008

DOI: 10.1016/j.earscirev.2008.04.004

2 authors, including:

Shuhab D Khan
University of Houston

Earth-Science Reviews 89 (2008) 135–143

Contents lists available at ScienceDirect

Earth-Science Reviews

journal homepage: www.elsevier.com/locate/earscirev

The application of remote sensing techniques to the study of ophiolites

Shuhab D. Khan [a,*], Khalid Mahmood [b]

[a] Department of Geosciences, University of Houston, Houston TX 77204, USA
[b] Center of Excellence in Mineralogy, University of Balochistan, Quetta, Pakistan

ARTICLE INFO

Article history:
Received 4 January 2008
Accepted 22 April 2008
Available online 10 May 2008

Keywords:
remote sensing
ASTER
ophiolite

ABSTRACT

Satellite remote sensing methods are a powerful tool for detailed geologic analysis, especially in inaccessible regions of the earth's surface. Short-wave infrared (SWIR) bands are shown to provide spectral information bearing on the lithologic, structural, and geochemical character of rock bodies such as ophiolites, allowing for a more comprehensive assessment of the lithologies present, their stratigraphic relationships, and geochemical character. Most remote sensing data are widely available for little or no cost, along with user-friendly software for non-specialists. In this paper we review common remote sensing systems and methods that allow for the discrimination of solid rock (lithologic) components of ophiolite complexes and their structural relationships. Ophiolites are enigmatic rock bodies which associated with most, if not all, plate collision sutures. Ophiolites are ideal for remote sensing given their widely recognized diversity of lithologic types and structural relationships. Accordingly, as a basis for demonstrating the utility of remote sensing techniques, we briefly review typical ophiolites in the Tethyan tectonic belt. As a case study, we apply integrated remote sensing studies of a well-studied example, the Muslim Bagh ophiolite, located in Balochistan, western Pakistan. On this basis, we attempt to demonstrate how remote sensing data can validate and reconcile existing information obtained from field studies. The lithologic and geochemical diversity of Muslim Bagh are representative of Tethyan ophiolites. Despite it's remote location it has been extensively mapped and characterized by structural and geochemical studies, and is virtually free of vegetative cover. Moreover, integrating the remote sensing data with 'ground truth' information thus offers the potential of an improved template for interpreting remote sensing data sets of other ophiolites for which little or no field information is available.

Contents

1. Introduction

Satellite data has radically improved our capabilities for imaging and mapping the earth's surface. Critical data bearing on topics such as global change, environmental geosciences, water quality and hydrology, mineral and petroleum exploration, volcanic, earthquake, flooding, and mass wasting hazards and detailed mapping in high-relief and remote areas are now available as a basis for a wide range of rigorous new insights. Remote sensing is highly effective in arid and semi-arid regions where geologic structures are extensively exposed. For example, ophiolite complexes offer excellent opportunities given the sensitivity of satellite-sensed data to their lithologic and structural diversity. Accordingly, this paper reviews applications of the most

* Corresponding author.
E-mail address: sdkhan@uh.edu (S.D. Khan).

0012-8252/$ – see front matter © 2008 Elsevier B.V. All rights reserved.
doi:10.1016/j.earscirev.2008.04.004

recently developed remote sensing techniques as a tool for mapping ophiolites. As a case study, we have selected the Muslim Bagh ophiolite, a relatively inaccessible but extensively studied ophiolite in western Pakistan in an attempt to integrate remote sensing data with 'ground truth' lithologic, structural, and geochemical information. Our ultimate objective is to develop tools for studying ophiolites (and other, analogous) bodies which due to topographic or other impediments are inaccessible for detailed field studies. Before describing remote sensing methodologies in detail, we present a brief resumé of some classic, well-studied ophiolites occurring in western Asia and the Himalayas, a largely arid region of the Tethyan tectonic belt.

2. The ophiolite 'conundrum'

The array of petrologic and structural features in western Tethyan ophiolites (e.g. Troodos, Semail, Oman, Mirdita, Albania) strongly supports the notion that most if not all represent fragments of former forearc complexes which resisted subduction due to their greater buoyancy relative to back-arc basin (MORB) crust. More significantly, these and most other ophiolites worldwide lack features that in any way preclude the forearc analogue. Virtually all 'complete' (i.e. fully exposed) ophiolites, consist of MORB-like basement lithologies and are characterized (along with some 'transitional' and calc-alkaline lithologies) by the structural attributes of seafloor spreading — sheeted dikes with 'one-way' chilling, 'fossil' transforms, and imbricated plutonic and pillow lava sequences, albeit in differing proportions. On the other hand, field relationships appear to indicate that the MORB-like lithologies largely pre-date the emplacement of boninites, high-Mg andesite (HMA), adakitic (plagiogranite), and calc-alkaline magmas. The notion that ophiolites represent petrologic 'signals' of subduction initiation events (e.g. Casey and Dewey, 1984; Stern and Bloomer, 1992) is supported by several features: 1) the relatively high-temperature (cf. MORB) magmas, showing unusually high Mg-numbers for equivalent MgO contents, superposing MORB basement, 2) the common presence of sub-ophiolitic metamorphic 'soles' — of MORB-like composition exhibiting strongly inflected, counterclockwise *P–T–t* metamorphic histories, and 3) the common presence of epidositic hydrothermal deposits (absent from active mid-ocean ridges). Together, these and other features suggest that 'proto-ophiolitic' forearc accretion involves splitting of the high-temperature 'proto-arc' and rapid arc–trench rollback, the denser back-arc basin crust being in most cases subducted ('basin collapse') prior to eventual collision of continental plates — e.g. fragments of north-drifting Gondwana with accreting Eurasia (Flower, 2003). Flower et al. (1998), Flower (2003) and Flower and Dilek (2003) have attributed such arc-forearc rollback episodes to mantle flow forces, reinforced by gravitational 'slab pull' forces inherent in subducting slabs.

Such models are supported by the petrologic, structural, and geochemical characteristics of the Tauride and near-contemporaneous Zagros ophiolites in Turkey (Parlak et al., 2002) and Iran (Ghazi et al., 2004), and indeed, further east in western Pakistan (Mahmood et al., 1995). However, the timing of the tectonic and magmatic evolution of the western end of the Himalayas is not well-understood, despite being integral to our understanding of the Himalayan orogeny. In this region, ophiolites also define an orogenic suture or sutures formed during the Late Cretaceous (Robertson, 2002; Mahmood et al., 1995). In contrast to the model outlined above, Tapponnier et al. (1981) argued that ophiolites in eastern Afghanistan and northwestern Pakistan

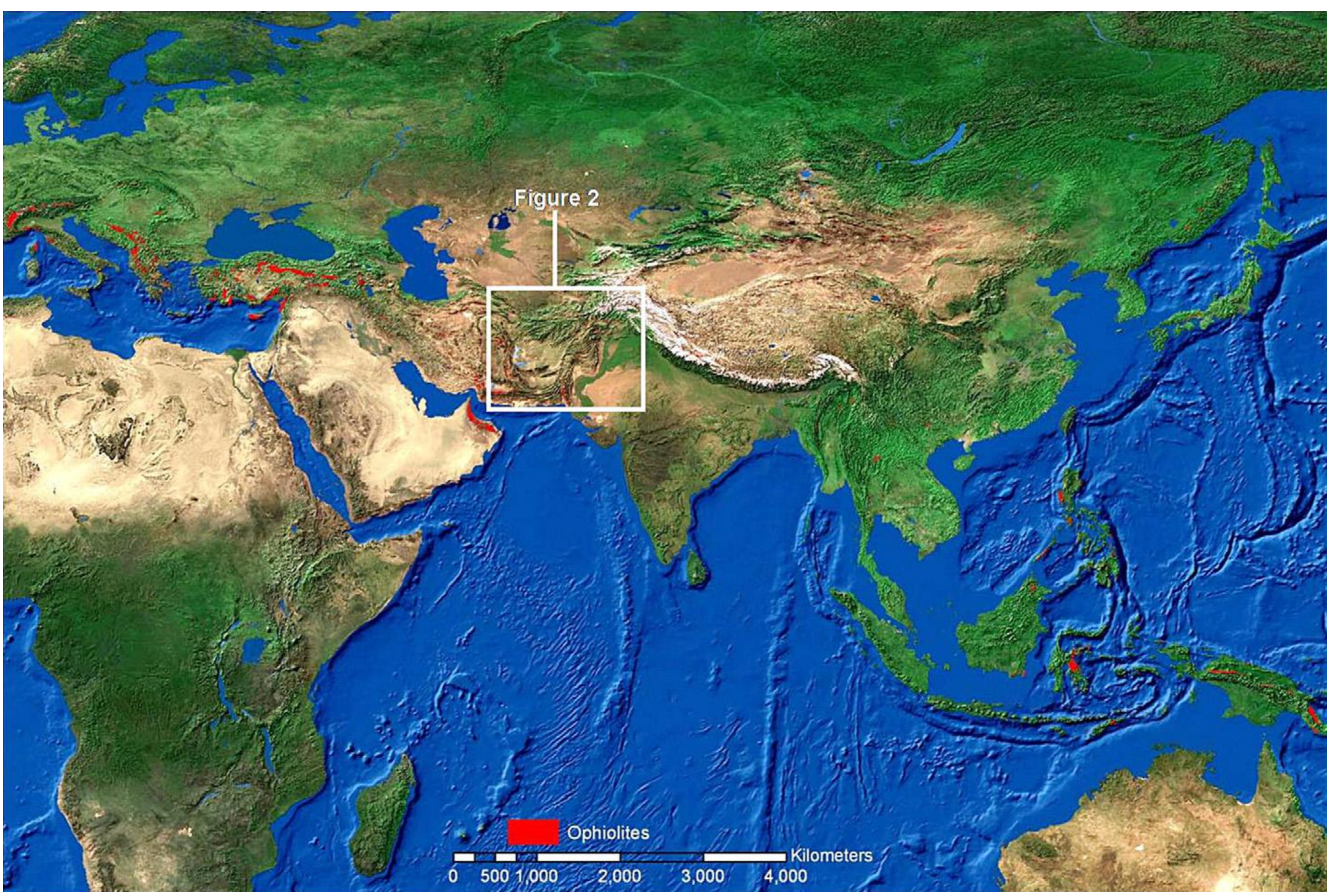

Fig. 1. MODIS image draped over digital elevation data showing location of ophiolites over Tethyan region (source of ophiolite locations; Khan et al., 2007b).

result from obduction of oceanic crust onto the Indian plate during the uppermost Cretaceous or Paleocene. In his scenario, this collision took place a few thousand kilometers away from the Asian continent (Tapponnier et al., 1981), a view followed by most other studies in the region (Searle 1986; Treloar and Izatt, 1993; Mahmood et al., 1995; Gnos et al., 1997). However, timing of the subsequent India–Asia collision is not well-constrained and has been placed between 55Ma (Klootwijk et al., 1991) and 45Ma (Dewey et al., 1989; Le Pichon et al., 1992), more recently than the eastern Mediterranean ophiolites (e.g. Robertson, 2002). A further complication may be that the Indian plate margin in western Pakistan did not collide with the Afghan block until the Late Pliocene (Treloar and Izatt, 1993). In any case, such models remain conjectural given the paucity of petrologic, geochemical, geochronologic, and structural studies of ophiolites in the region, all of which are contingent on detailed mapping of lithologies present and their stratigraphic relationships.

3. Muslim Bagh — a case study

The present review, it is hoped, will mitigate the latter problem. This paper describes the efficacy of remote sensing as an aid to mapping in one of the few exceptions, the Muslim Bagh ophiolite, in Balochistan, western Pakistan, which has been the focus of detailed mapping and sampling over a period of many years (e.g. Mahmood et al., 1995, and refs. therein). Better constraints on the genesis and timing of this and other ophiolites will be critical to interpreting collision dynamics in western Pakistan in the broader context of neo-Tethyan closure and the Himalayan orogeny. The Muslim Bagh ophiolite (MBO) is best exposed in Pakistan and represents a classic, near-complete ophiolitic sequence, lacking only the uppermost extrusive and sedimentary components.

The MBO lies east-northeast of Quetta (Fig. 2) and comprises two main blocks, Jang Tor Ghar (JTG) and Saplai Tor Ghar (STG). The mantle sections of both these blocks consist of alternating harzburgite and dunite bands. The dunite hosts podiform chromite that occurs as irregular bodies ranging in size from tens to hundreds of meters and is mined commercially. The best preserved subophiolitic metamorphic sole rocks are located along the northwestern side of the JTG and show inverted metamorphic gradients. The series starts at the contact with peridotite mylonites and garnet amphibolites and grades downwards into amphibolites and fine-grained epidote amphibolites or greenschists. Garnet amphibolites occur at the immediate contact with mylonitzed peridotites (Rossman et al., 1971; Munir and Ahmad, 1985; Mahmood et al., 1995). Highly depleted coarse grained residual harzburgites and dunites lie above basal mylonitized peridotite. An ultramafic-mafic transition zone is followed upward by gabbroic rocks. The crustal section consists of layered and foliated gabbroic rocks, isotropic gabbros and a sheeted dike complex. Typical pillow lava sequences are missing and presumably eroded. A large number of dolerite dikes cut the STG block, whereas few dikes are present in the JTG (Mahmood et al., 1995). At places, the dikes grade into gabbro or pyroxenite bodies. The dolerite dikes are generally a few meters to ~500 m in thickness. On the basis of field studies, Sillitoe (1978) and Otsuki et al. (1989) interpreted that this ophiolite complex was formed in an oceanic ridge setting in the Neo-Tethys. Khan et al. (2007a) suggest a combination of mid-oceanic ridge, hot spot and subduction zone magmatism in MBO.

Mahmood et al. (1995) reported a 65–70Ma age for MBO based on $^{40}Ar/^{39}Ar$ ages from the sub-ophiolitic metamorphic sole and amphibole from the base of a sheeted dike complex. We interpret this age to represent the approximate cooling age of the metamorphic sole and mantle detachment, which places a minimum age on the formation of the ophiolite complex as a whole. Based on structural studies of the MBO and related metamorphic rocks, Mahmood et al. (1995) interpreted the MBO as a segment of ocean floor that was emplaced onto India during the convergence of neo-Tethys prior to the Indo-Asian collision.

4. Mapping ophiolites by remote sensing

Many satellites are orbiting or have orbited Earth; broadly these could be grouped into two categories, environmental and earth resources satellites. Environmental satellites monitor environmental conditions with swath widths of 100s of km (coarse resolution). Use of environmental satellites is not common in geology but holds potential for regional and global applications. For example the Moderate Resolution Imaging Spectro-Radiometer (MODIS) instrument is the primary sensor collecting data for global-change monitoring on both the Terra and Aqua satellites. With its 2330 km-wide swath, the MODIS sensor provides one to two-day coverage of earth in 36 spectral bands at spatial resolutions of 250m, 500m and 1 km. These data are available free of cost. Fig. 1 shows a MODIS image draped over digital elevation data showing major ophiolite bodies in the Tethyan region.

Earth resources satellites map renewable and non-renewable resources (along with other applications) with swath widths<200 km (fine resolution). Earth resource satellites include sensors like Landsat,

Table 1
Technical specification of MODIS, ASTER, Landsat ETM+, SPOT 5 and IKONOS

MODIS			ASTER			Landsat ETM+			SPOT 5			IKONOS		
Band #	Spectral range (μm)	Ground resolution (m)	Band #	Spectral range (μm)	Ground resolution (m)	Band #	Spectral range (μm)	Ground resolution (m)	Band #	Spectral range (μm)	Ground resolution (m)	Band #	Spectral range (μm)	Ground resolution (m)
1	0.620–0.670	250	1	0.52–0.60	15	1	0.450–0.515	30	1	0.5–0.59	10	1	0.45–0.53	4
2	0.841–0.876	250	2	0.3–0.69	15	2	0.525–0.605	30	2	0.61–0.68	10	2	0.52–0.61	4
3	0.459–0.479	500	3N	0.76–0.86	15	3	0.630–0.690	30	3	0.78–0.89	10	3	0.64–0.72	4
4	0.545–0.565	500	3B	0.76–0.86	15	4	0.750–0.900	30	4	1.58–1.75	20	4	0.77–0.88	4
5	1.230–1.250	500	4	1.60–1.70	30	5	1.55–1.75	30						
6	1.628–1.652	500	5	2.145–2.185	30	7	2.09–2.35	30						
7	2.105–2.155	500	6	2.185–2.225	30	6	10.4–12.5	60						
8–16	0.405–0.965	1000	7	2.235–2.285	30	Pan	0.520–0.900	15	Pan	0.48–0.71	2.5–5.0	Pan	0.45–0.90	1
17–19	0.890–0.965	1000	8	2.295–2.365	30									
20–25	3.66–4.459	1000	9	2.360–2.430	30									
26	1.36–1.39	1000	10	8.125–8.475	90									
27–29	6.535–8.7	1000	11	8.475–8.825	90									
30–33	9.58–13.485	1000	12	8.925–9.275	90									
34–36	13.485–14.385	1000	13	10.25–10.95	90									
			14	10.95–11.65	90									
Swath width: 2330 km			Swath width: 60 km			Swath width: 185 km			Swath width: 60 km			Swath width: 11 km		
Coverage interval: 1–2 days			Coverage interval: 16 days			Coverage interval: 16 days			Coverage interval: 26 days			Coverage interval: 1.5–3 days		
Altitude: 705 km			Altitude: 705 km			Altitude: 705 km			Altitude: 832 km			Altitude: 681 km		

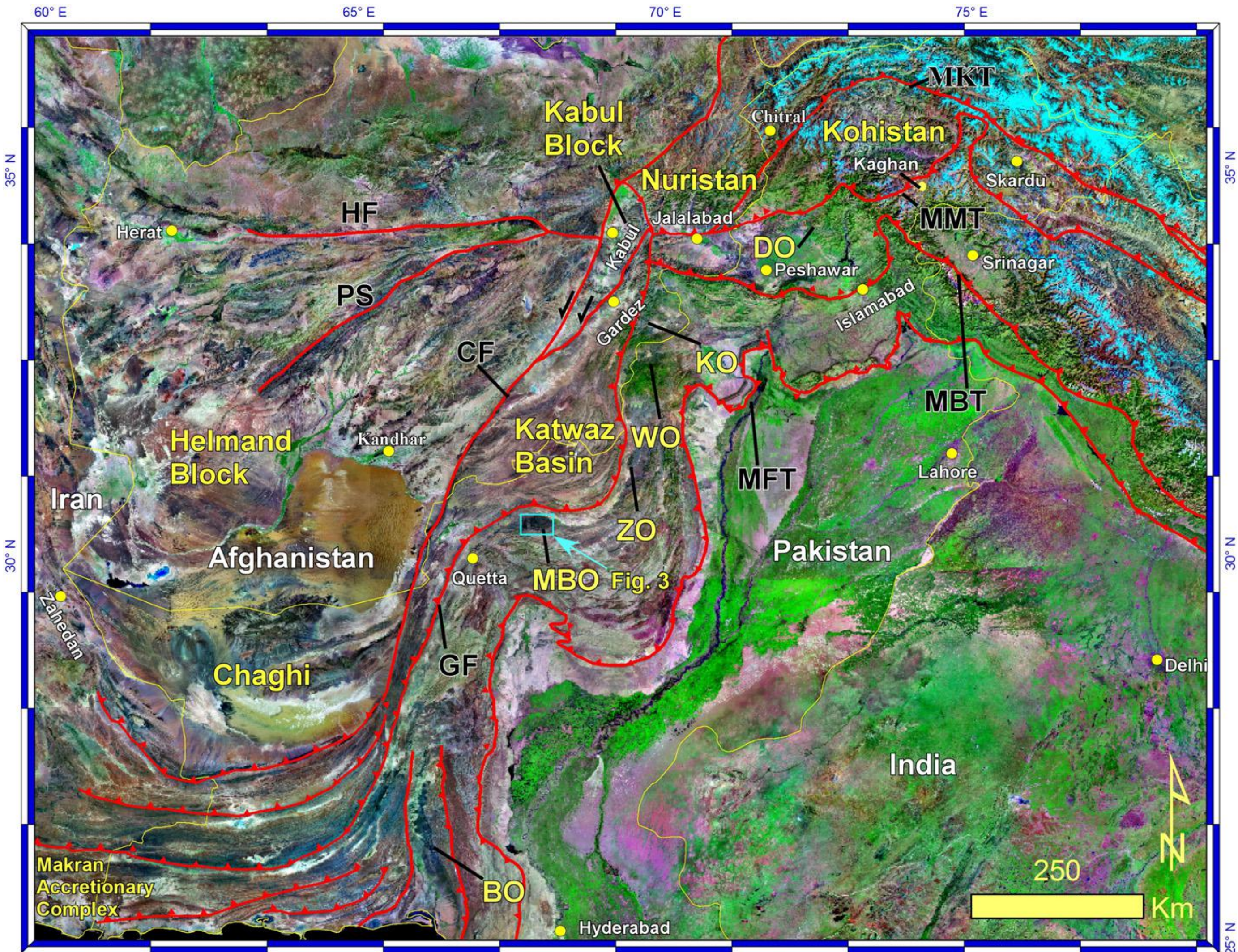

Fig. 2. Landsat satellite image showing tectonic sketch map of southeast Asia. Faults and sutures are drawn from Yin (2006), Tapponnier et al. (1981), Lawrence et al. (1981), and Gaetani et al. (2004). BO = Bela Ophiolite; MBO = Muslim Bagh Ophiolite; ZO = Zhob Ophiolite; WO = Waziristan Ophiolite; KO = Khost Ophiolte; DO = Dargai Ophiolite; GF= Ghazband Fault; CF = Chaman Fault; PF = Panjao Shear; HF = Heart Fault; MFT = Main Frontal Thrust; MBT = Main Boundary Thrust, MMT = Main Mantle Thrust; MK = Main Karakoram Thrust.

SPOT, ASTER, IKONOS, etc., and are routinely used in geological applications. Table 1 shows the summary of spectral and spatial resolution for common remote sensing sensors. With the advent of Google Earth it is common to download an image and use it as a background over which vector data can be displayed in Geographic Information System (GIS) software or other applications. Also, NASA's 2000 GeoCover global orthorectified Landsat 7 mosaics are available free of cost as color-composite MrSID files from https://zulu.ssc.nasa.gov/mrsid. Each of the MrSID files contains a 24-bit color image with Band 7 as red, Band 4 as green, and Band 2 as blue. Each file spans the six-degree width of a Universal Transverse Mercator (UTM) zone and covers 5° of latitude, with a cell size of 14.25m. This scale is very useful in mapping the extent of an ophiolite; for example, Fig. 2 shows major ophiolites in western Pakistan.

Detailed lithological discrimination requires advanced digital image processing techniques. For example, raw data received from remote sensors often contains flaws and requires enhancements to allow for extraction of information. Image processing requirements vary from image to image, depending on the type of data, initial condition of the image, and the type of information of interest. Digital image processing is typically applied on raster data, and each image is treated as an x, y array of digital numbers. We summarize here image processing techniques applicable for ophiolite mapping.

Rothery (1987) distinguished lavas, sheeted dikes and mantle sequence in the Oman ophiolite using Landsat Thematic Mapper TM color-composite image using bands 7, 5 and 4. Sultan et al. (1987) identified the following sets of TM bands ratio for mapping serpentinites in the Eastern Desert of Egypt; (1) TM band 5/1 to emphasize overall variations due to opaque mineral content; (2) band 5/7 to emphasize variations in content of hydroxyl-bearing minerals; and (3) bands 5/4 X 3/4 to emphasize variations related to ferrous electronic transition bands in silicates (e.g., amphiboles) near 1.0 µm. Decorrelation stretching of these bands (Landsat TM, 7–5–4) was found effective in mapping plutonic lithologies of the Oman ophiolite (Abrams et al., 1988). Chevrel et al. (1991) used geometrically and radiometrically corrected SPOT data and recognized sheeted dikes, gabbros and trondhjemites in the Semail ophiolite of Oman. Utke and Siad (1993) showed the utility of Landsat TM Bands 7–4–1 for identification of island arc and ophiolite rocks in Red Sea Hills, Sudan. In 1992 JERS-1 was launched by the National Space Development Agency (NASDA) of Japan. JERS-1 has better spatial and spectral resolution than Landsat TM. Using JERS-1 data Denniss et al. (1994) were able to map more precisely the lithological boundaries within the sequence from harzburgite to layered gabbros in the Oman ophiolite. Using Spectral Angel Mapper (SAM) techniques on Landsat TM data, Van der Meer et al. (1997) were able to recognize a boundary between two

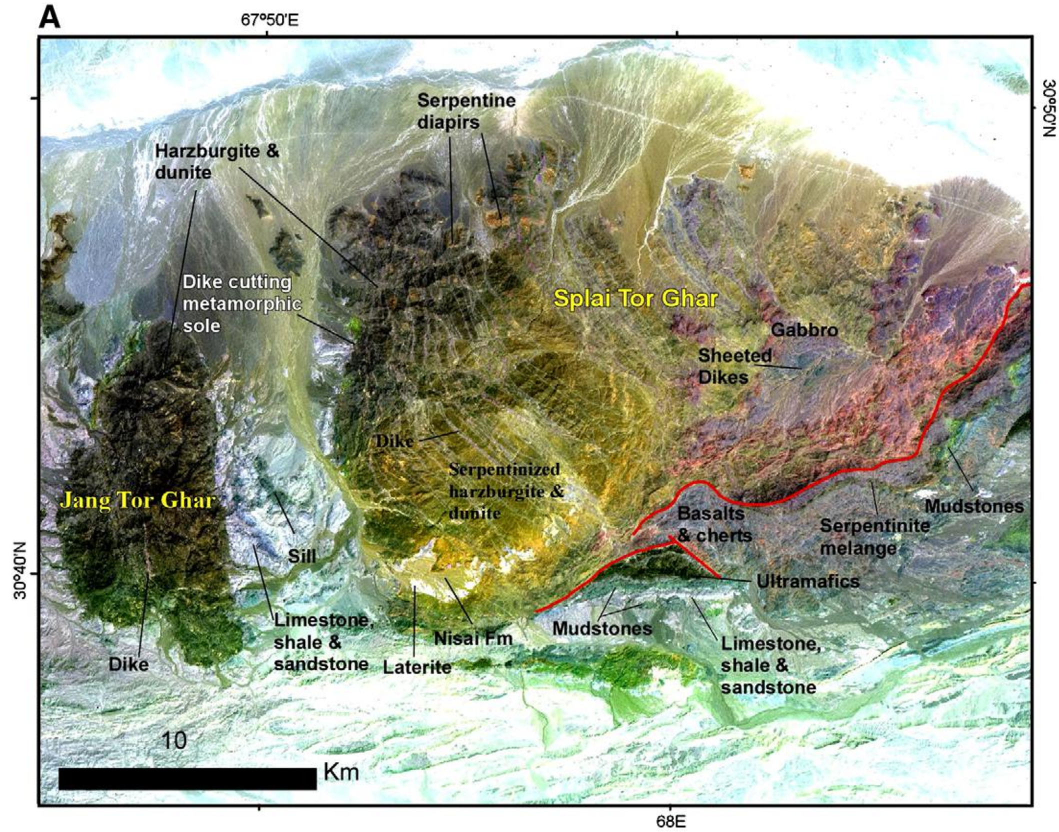

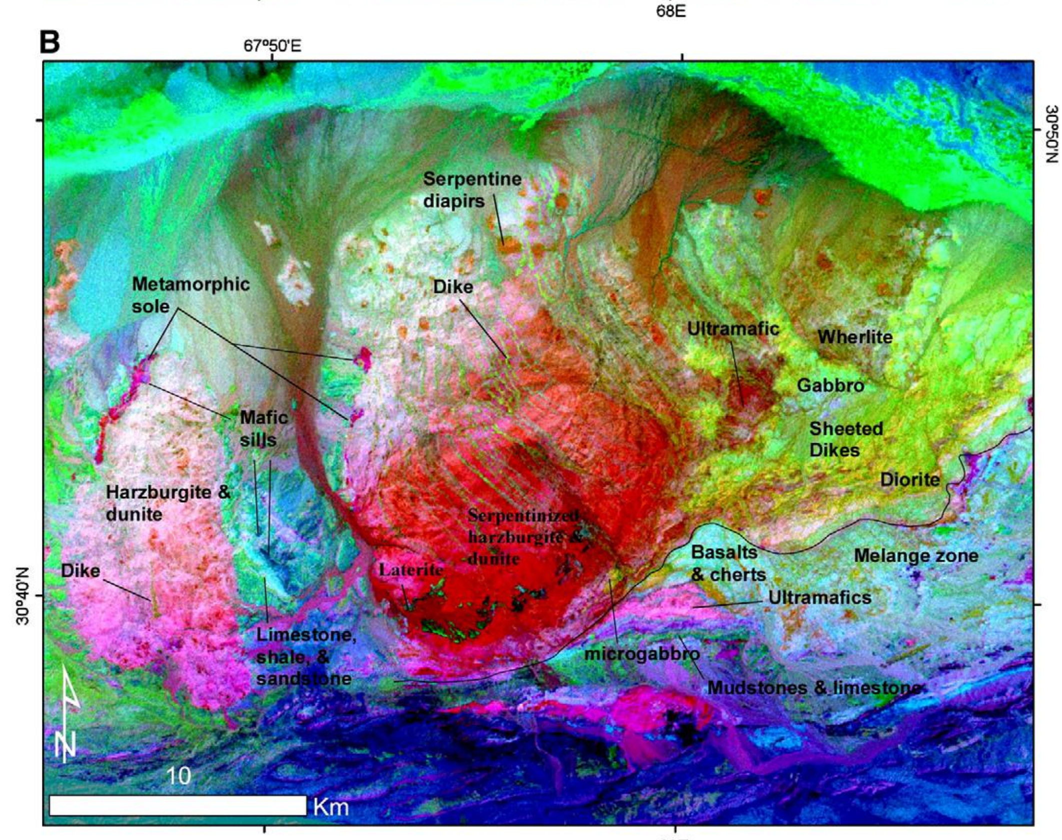

Fig. 3. (A) Log residual applied ASTER SWIR bands 4, 5 and 8 are displayed as red, green and blue respectively. This combination discriminates serpentinized harzburgite and dunite from unaltered harzburgite and dunite dikes, gabbros, basalt and sedimentary units of MBO. (B) ASTER MNF transformed bands 1, 2 and 3 are displayed as red, green and blue respectively. This image shows enhanced metamorphic sole, peridotites and serpentinites, diorite and limestone. (C) spectral reflectance curves for dunite, gabbro, diabase, basalt, serpentinite and sandstone (source Korb et al., 1996).

lava types that form a zone for copper mineralization. They were also able to identify serpentinized dunites that may be hosting asbestos deposits.

The Advanced Spaceborne Thermal Emission and Reflection Radiometer (ASTER) instrument was developed by NASDA and launched by National Aeronautics and Space Administration (NASA) on the Terra

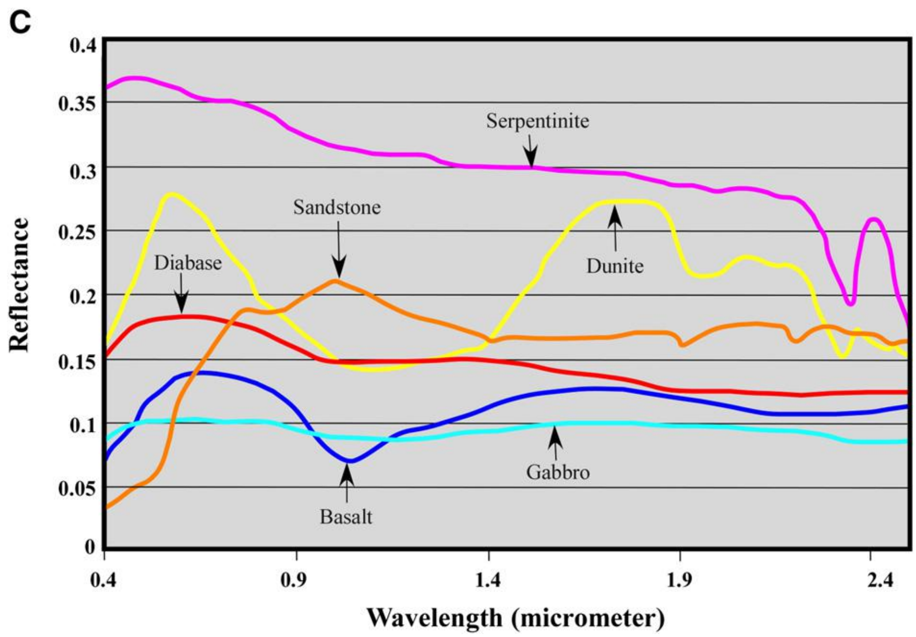

Fig. 3 (*continued*).

satellite in December 1999 as part of NASA's Earth Observing System (EOS). It provides three bands (not including the backward-looking telescope in Band 3 for digital stereo-pair/DEM generation) in the visible to near infrared (VNIR) at 15m resolution, six bands in the short-wave infrared (SWIR) at 30m resolution, and five bands in the thermal-infrared (TIR) at 90m resolution. The ASTER data have 60 km-wide swaths. ASTER provides better spatial and spectral resolution than Landsat TM data (see Table 1). Ninomiya (2003) looked at spectral features of different minerals in ASTER data and formulated the following mineral indices:

OH bearing altered mineral index (OHI) = (Band 7 / Band 6) × (Band 4 / Band 6)
Kaolinite Index (KLI) = (Band 4 / Band 5) × (Band 8 / Band 6)
Alunite Index (ALI) = (Band 7 / Band 5) × (Band 7 / Band 8)
Calcite Index (CLI) = Band 6 / Band 8) × (Band 9 / Band 8).

These indices were applied to ASTER Level-1B radiance at the sensor scenes in the Cuprite district in Nevada, USA, and this technique holds potential for mapping ophiolite lithologies. Using ASTER Thermal Infrared (TIR) data, Ninomiya et al. (2005) also suggested the Quartz Index (QI), Calcite Index (CI), and Mafic Index (MI), where QI = (Band 11 × Band 11) / (Band 10 × Band 12), CI = (Band 13 / Band 14), and MI = (Band 12 / Band 13). These techniques were applied to areas in China and Australia, and the results indicated that these indices discriminate quartz, carbonate and mafic-ultramafic rocks. Rowan et al. (2005) used ASTER data to map the Mordor complex, Australia, which consists of potassic mafic-ultramafic rocks. It was found that band ratio images provided a quick method for distinguishing lithologies. However, SAM and matched-filter processing of VNIR and SWIR data provided more lithological information. Khan and Glenn (2006) used decorrelation stretches, principal components analyses, and SAM classifications techniques on ASTER data and created a lithologic and structural map at 1:250 000 scale for northern Pakistan.

5. Remote sensing results from Muslim Bagh

Preliminary maps of the MBO based on remote sensing and field observations were created by Khan et al., 2007b. In this paper, we augment these results and show, on the basis of field studies, the extent to which the principal lithologies can be recognized from the remote sensing data. This information can be used as a basis for further sampling for geochemical and other sample-based studies. To characterize the significance of dolerite and sheeted dikes and to highlight the other lithologic units, ASTER satellite images were further processed for use in this study. We investigated a single ASTER image acquired at April 10, 2006 over the MBO. Short-wave infrared (SWIR) bands provide better results for discriminating lithology of the ophiolite (e.g., Rowan et al., 2005; Khan and Glenn, 2006). Image data was processed using ENVI 4.4 software. A log residual algorithm was applied to the SWIR data, and the data were spatially sharpened to 15m. The log residual algorithm reduces noise from topography, instrument and sun illumination (Green et al., 1988) using the formula:

$$(B1*mean(B2))/(B2*mean(B1))$$

where B1 = SWIR bands 1 to 6; B2 = average band calculated from 6 SWIR bands; mean = arithmetic mean.

We applied log residual algorithm to all SWIR bands. The color-composite bands 4–5–8 image of the log residual data is shown in Fig. 3A. The processed ASTER data were able to discriminate most of the lithologies. The harzburgite and dunite are dark due to the presence of opaque minerals (i.e., chromites). Field observations show that harzburgites form massive bodies and is the most common ultramafic rock in the study area. It can be easily recognized in the field by its "hob-nail" outcrops. It generally shows serpentinization. The fresh surface is greenish black, but the color of the weathered surface is dark brown to brownish. They are medium to coarse grained and porphyroclastic to mylonitic at places (Fig. 4A). Dunites are the second most abundant ultramafic rocks, dunites are composed essentially of olivine and spinel (1–2%). Many outcrops of dunites have the large concentration of chromites, which are being mined locally in the areas. The structures in these chromite bodies are concordant to host rock (dunite). Serpentines and serpentinized ultramafics are red or reddish due to hydrous minerals like antigorite and chrysotile, which have bright reflection in band 4 and show vibrational bands and OH-stretching near 2.1µm (Fig. 3C). Serpentinite diapirs were confirmed in the field (Fig. 4B). The serpentinites in these bodies are composed of more than 90% of serpentine with the remaining minerals are opaque (spinel and magnetite) and olivine. The serpentine vary in color from light green to brownish green. Eighty to ninety percent of the peridotites of the study area are serpentinized (Fig. 3). The massive serpentinization had affected principally the dunites. Diabase dikes/sills show alteration minerals like epidote, which is dominated by OH related bands at 2.35µm. Rocks in these dikes/sills are dark grey to greenish grey. On both sides of the dikes, the rocks show serpentinization and chilled margins. The thickness of these dikes varies from meters to centimeters. The mélange zone contains blocks of ultramafic and mafic rocks in a serpentine matrix, this zone also shows thick basalt and sedimentary rocks (Fig. 5). Basalt and sheeted dikes also appear dark, probably because of opaque minerals like magnetite.

The minimum noise fraction (MNF) transform is used to determine the inherent dimensionality of the image data to segregate noise in the data and to reduce the computational requirements for subsequent processing (Boardman et al., 1995). MNF involves two steps; in first step which is also called noise- whitening, principal components for noise covariance matrix are calculated, this step decorrelates and rescales the noise in the data. In second step principal components are derived from the noise whitened data. The data can then be divided into two parts: one part associated with large eigen values and the other part with near-unity eigen values and noise-dominated images. Using data with large eigen values separates the noise from the data, and improves spectral results (Green et al., 1988). The MNF transformation was applied to the ASTER data which enhanced the metamorphic sole, peridotites and serpentinites, diorite, and limestone (Fig. 3B). The 4th and 5th MNF components were mostly noisy images and do not enhance any rock

A

B

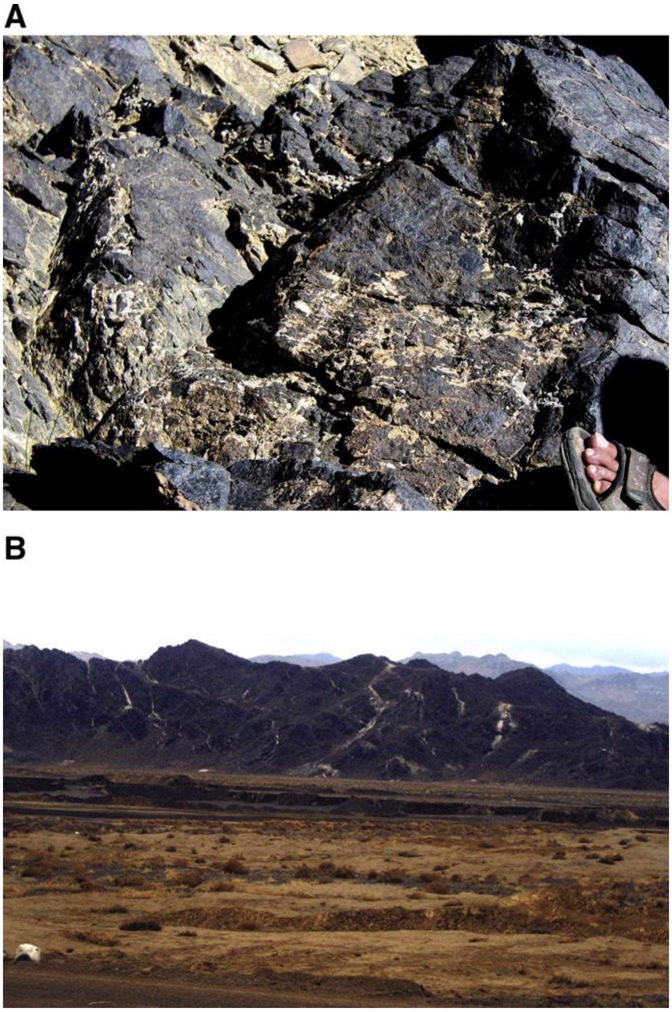

Fig. 4. (A) Field photograph showing the unaltered harzburgite in Jang Tor Ghar body of the Muslim Bagh Ophiolite. (B) A serpentine diapir northern side of the Spalai Tor Ghar block.

A

B

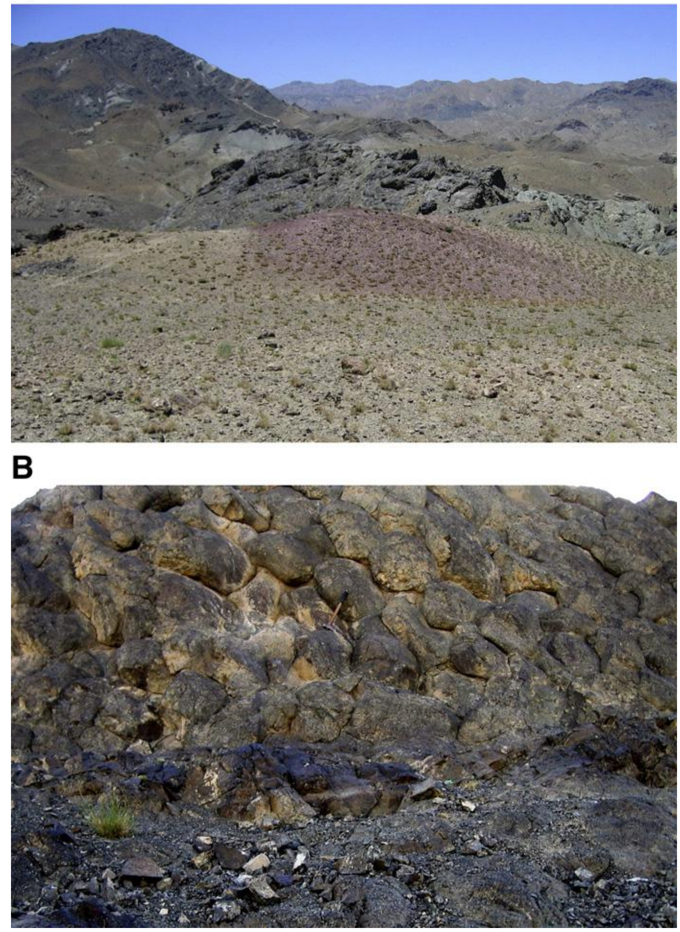

Fig. 5. (A) Colored mélange below the Saplai Tor Ghar block. (B) View of pillow basalts cut by diabase dike. The pillow lava show minor limestone intercalations.

unit. Remote sensing interpretations were confirmed during our field work in 2006. Our work reveals the presence of a large number of dolerite dikes and sills cutting the mantle rocks; these rocks also cut the metamorphic sole and the mélange zone. Our data illustrate existence of serpentinite diapirs and the extent of the sheeted dike complex.

6. Discussion

Ophiolites have been interpreted as relict fragments of crust formed at ocean ridges, marginal basins, mantle plume loci, and volcanic arcs (e.g., Moores, 1982; Casey and Dewey, 1984; Nicolas et al., 1988). However, many of these bodies may represent buoyant, intra-oceanic forearc remnants, entrapped either by initiation of intra-oceanic subduction or by arc polarity flips after plate collisions following the collapse of back-arc basins (Casey and Dewey, 1984; Stern and Bloomer, 1992; Shervais, 2003; Flower et al., 2001; Flower and Dilek, 2003). This interpretation implies a linkage between pre-collision initiation of subduction as subduction on rollback cycles and abrupt regional plate kinematic changes (Casey and Dewey, 1984; Stern and Bloomer, 1992; Flower et al., 2001; Flower and Dilek, 2003). To resolve such questions well-constrained geochemical, structural, and geochronologic studies will be essential and, furthermore, contingent on detailed mapping of lithologies present and their structural and stratigraphic relationships.

In the case of the MBO, the petrology and geochemistry of the sheeted dike complex and dolerite dikes favor a forearc origin for the MBO (Khan et al., 2007b).

The features identified by the remote sensing data in well-studied ophiolites can be used as a key to distinguish tectonic settings of the ophiolites. For example indicative forearc lithologies include MORB basement, a boninitic proto-arc, rocks with continental components (Flower, 2003), serpentinite mud diapirs (Fryer et al., 2000), and high temperature hydrothermal deposits. Also boninites are more common in ophiolites than previously thought (e.g. Flower, 2003), and are reported from the 'crescent' ophiolites: Mersin, Pozanti–Karsanti, and Hatay–Kizildag (Parlak et al., 1996; Polat et al., 1996, Lytwyn and Casey, 1993, 1995), Baer–Bassit (Al-Riyami et al., 2000), and the central Tauride Divrigi and Kuluncak mélanges and Sarikaraman ophiolite (Yalınız et al., 2000). The Hatay–Kizildag ophiolite strongly resembles Troodos (Cyprus) and was ascribed by Lytwyn and Casey (1993) to extension in forearc settings following intra-oceanic compression and subduction nucleation. In the case of Pozanti–Karsanti, a short distance to the northwest, sheeted mantle tectonites and MORB-like cumulates, isotropic gabbros, dikes, and lavas are cut by dikes at all structural levels (Lytwyn and Casey, 1993) while gabbroic cumulates likewise show extreme low-Ti clinopyroxenes. None of the dike samples from Muslim Bagh are boninites, but data for mineral separates (Cpx, Ol, and spinel) can provide a basis for classifying magmatic affinity (e.g., Parlak et al., 1996). Chromium (Cr)-number [100 * Cr / (Cr + Al)], Mg-number ([100 * Mg / (Mg + Fe^{+2}]), and Cr-number and TiO_2 provide good discriminators of boninite, calc-alkaline, and MORB-like magmas (Arai et al., 1997; Ahmed et al., 2001; Pearce, 2003). Parlak and Delaloye (1999) showed that some of the chromites from the Pozanti–Karsanti ophiolite and basal cumulates of the Mersin ophiolite have boninitic affinities. Likewise, spinels from the MBO have compositions that indicate a boninitic source for the magma (Khan et al., in review). Additional arguments in favor of a forearc setting for MBO include the dispersed serpentinite bodies in the MBO (Fig. 3) that we consider as serpentinite diapirs. Fryer et al. (2000) suggested that these dispersed serpentine bodies in a convergent zone could be similar to the present-day mud volcanoes of the Mariana forearc. Also, high temperature hydrothermal deposits are another feature of fore-arc settings, and several small-scale hydrothermal deposits of copper are present in the mélange zone and in ultramafic and gabbroic rocks of the MBO (Nakagawa et al., 1996).

7. Conclusion

Rapid advances in remote sensing and digital image processing techniques offer unprecedented opportunities for researchers to study and map ophiolites at different scales and details. The example of the MBO provides an excellent opportunity to demonstrate the utility of ASTER remote sensing data for discriminating ophiolite lithologies — e.g., harzburgite, lherzolite, dunite, diabase dikes and sills, serpentinites, basalt and sediments.

Processed ASTER data show serpentinite diapirs and large numbers of dolerite dikes and sheeted dikes in the Muslim Bagh ophiolite. Geochemical data of the mafic rocks from the sheeted dike complex and dolerite dikes in the MBO (discussed more fully by Khan et al., in review) show negative Nb, Ta, Hf and Zr anomalies, signifying a subduction-related origin for the rocks. These rocks also show Th enrichment and Ta depletion suggesting variable addition of subduction components to a heterogeneous mantle wedge. Tholeiitic to calc-alkaline chemistry, the presence of boninitic magmas, high temperature hydrothermal deposits, and serpentinite diapirs imply a forearc setting for the formation of Muslim Bagh ophiolite. This forearc is interpreted to have been part of a large Cretaceous intra-oceanic island arc system, which included the Kohistan and Ladakh arcs. This intra-oceanic arc is interpreted to have collided with the northern margin of India around 65Ma in low northern latitudes prior to final closure of the Tethys.

Acknowledgements

The Institute of International Education funded Mahmood's visit to the University of Houston and University of Illinois at Chicago as Fulbright Scholar and the Commonwealth Foundation sponsored his visit to Cardiff University as Postdoctoral Fellow. We also want to thank Dr. John F. Casey, Julia Wellner, Alex Robinson and Rosalie Maddocks for their help. We thank Dr. A. Salam Khan, CEM, University of Balochistan for his support.

References

Abrams, M.J., Rothery, D.A., Pontual, A., 1988. Mapping in the Oman Ophiolite using enhanced Landsat thematic mapper images. Tectonophysics 151, 387–401.

Ahmed, A.H., Arai, S., A., Attia, K., 2001. Petrological characteristics of podiform chromitites and associated peridotites of the Pan African Proterozoic ophiolite complexes of Egypt. Mineralium Deposita 36, 72–84.

Al-Riyami, K., A., Robertson, H.F., Xenophontos, C., Danelian, T., Dixon, J.E., 2000. Tectonic evolution of the Mesozoic Arabian passive continental margin and related ophiolite in Baer–Bassit region (N W Syria). In: Panayides, I., et al. (Ed.), Proceeding of 3rd International Conference on the Geology of the Eastern Mediterranean, 17. Geological Survey Department, Cyprus, pp. 24–25.

Arai, S., Kadoshima, K., Manjoorsa, K.V., David, C.P., Kida, M., 1997. Chemistry of detrital chromium spinels as an insight into petrological characteristics of their source peridotites; an example from the Ilocos Norte Ophiolite, northern Luzon, Philippines. Journal of Mineralogy, Petrology and Economic Geology 92 (4), 137–141.

Boardman, J.W., Kruse, F.A., Green, R.O., 1995. Mapping target signatures via partial unmixing of AVIRIS data. In: Jakob, V.Z. (Ed.), Summaries of the Fifth JPL Airborne Earth Science Workshop, 3. J. P. L, Pasadena, CA, pp. 23–26.

Casey, J.F., Dewey, J.F., 1984. Initiation of subduction zones along transform and accreting plate boundaries, triple-junction evolution, and forearc spreading centers; implications for ophiolitic geology and obduction. In: Gass, I.G., et al. (Ed.), Ophiolites and Oceanic Lithosphere. Geol. Soc. Lond. Spec. Publ., vol. 13, pp. 269–290.

Chevrel, S., Chevremont, P., Wyns, R., Le Metour, A., Toba, A., Beurrier, M., 1991. The use of digitally processed SPOT data in the geological mapping of the ophiolite of northern Oman. In: Peters, T.J. (Ed.), Ophiolite Genesis and Evolution of the Oceanic Lithosphere, pp. 853–870.

Denniss, A.M., Rothery, D.A., Ceuleneer, G., Amri, I., 1994. Lithological discrimination using Landsat and JERS-1 SWIR data in the Oman Ophiolite. Proceedings of the Tenth Thematic Conference on Geologic Remote Sensing: Exploration, Environment, and Engineering, San Antonio, Texas, USA, pp. II–97–II-107.

Dewey, J.F., Cande, S., Pitman, W.C., 1989. Tectonic evolution of the India/Eurasia collision zone. Eclogicae Helveta 82, 717–734.

Flower, M.F.J., Russo, R.M., Tamaki, K., Hoang, N., 2001. Mantle contamination and the Izu–Bonin–Mariana (IBM) "high-tide mark"; evidence for mantle extrusion caused by Tethyan closure. Tectonophysics 333, 9–34.

Flower, M.F.J., 2003. Ophiolites, historical contingency, and the Wilson Cycle. In: Dilek, Y., Newcomb, S. (Eds.), Ophiolite Concept and the Evolution of Geological Thought. GSA Spec. Publ, vol. 73, pp. 111–136.

Flower, M.F.J., Dilek, Y., 2003. Arc–trench rollback and forearc accretion: a collision-induced mantle flow model for Tethyan ophiolites. In: Dilek, Y., Robinson, P.T. (Eds.), Ophiolites in Earth History. Geological Society of London Special Publication, vol. 18, pp. 21–41.

Flower, M.F.J., Tamaki, K., Hoang, N., 1998. Mantle extrusion; a model for dispersed volcanism and DUPAL-like asthenosphere in East Asia and the western Pacific. In: Flower, M.F.J., Chung, S.L., Lo, C.H., Lee, T.Y. (Eds.), Mantle Dynamics and Plate Interactions in East Asia. Am. Geophys. Union Geodynamics Series, 27, pp. 67–88.

Fryer, P., Lockwood, J.P., Becker, N., Phipps, S., Todd, C.S., 2000. Significance of serpentine mud volcanism in convergent margins. In: Dilek, Y., et al. (Ed.), Ophiolites and Oceanic Crust: New Insights from Field Studies and the Ocean Drilling Program. Geological Society of America Special Paper, vol. 349, pp. 35–51.

Gaetani, M., Zanchi, A., Angiolini, L., Olivini, G., Sciunnach, D., Brunton, H., Nicora, A., Mawson, R., 2004. The Carboniferous of western Karakoram (Pakistan). J. Asian Earth Sci. 23, 275–305.

Ghazi, A.M., Hassanipak, A.A., Mahoney, J.J., Duncan, R.A., 2004. Geochemical characteristics, ^{40}Ar–^{39}Ar ages and original tectonic setting of the Band-e-Zeyarat/Dar Anar ophiolite, Makran accretionary prism, S.E. Iran. Tectonophysics 393, 175–196.

Gnos, E., Immenhauser, A., Peters, T., 1997. Late Cretaceous/early Tertiary convergence between the Indian and Arabian plates recorded in ophiolites and related sediments. Tectonophysics 271 (1–2), 1–19.

Green, A.A., Berman, M., Switzer, P., Craig, M.D., 1988. A transformation for ordering multispectral data in terms of image quality with implications for noise removal. IEEE Trans. Geosci. Remote Sens. 26 (1), 65–74.

Klootwijk, C.T., Gee, J.S., Peirce, J.W., Smith, G.M., Guy, M., 1991. Constraints on the India–Asia convergence; paleomagnetic results from Ninetyeast Ridge. Proceedings of the Ocean Drilling Program. Scientific Results, vol. 121, pp. 777–882.

Khan, S.D., Glenn, N., 2006. New strike slip faults and litho-units mapped in Chitral (N. Pakistan) using field and ASTER data yield regionally significant results. Int. J. Remote Sens. 27 (2), 4495–4512.

Khan, M., A., Kerr, C., Mahmood, M., 2007a. Formation and tectonic evolution of the Cretaceous–Jurassic Muslim Bagh ophiolitic complex, Pakistan: implications for the composite tectonic setting of ophiolites. J. Asian Earth Sci. 31 (2), 112–127.

Khan, S.D., Mahmood, K., Casey, J.F., 2007b. Mapping of Muslim Bagh ophiolite complex (Pakistan) using new remote sensing, and field data. J. Asian Earth Sci. 30, 333–343.

Khan, S. D., Walker, D. J., Hall, S., Stockli, L., and Shah, M. T., (in review), Did Kohistan collide first with India? GSA Bull.

Korb, A.R., Dybwad, P., Wadsworth, W., Salisbury, J.W., 1996. Portable FTIR spectrometer for field measurements of radiance and emissivity. Appl. Opt. 35, 1679–1692.

Lawrence, R.D., Khan, S.H., DeJong, K.A., Farah, A., Yeats, R.S., 1981. Thrust and strike slip fault interaction along the Chaman transform zone, Pakistan. In: McClay, K., Price, N. (Eds.), Thrust and Nappe Tectonics. Geol. Soc. Lond. Sp. Pub., vol. 9, pp. 363–368.

Le Pichon, Fournier, X.M., Jolivet, L., 1992. Kinematics, topography and extrusion in the India–Eurasia collision. Tectonics 11, 1085–1098.

Lytwyn, J.N., Casey, J.F., 1993. The geochemistry and petrogenesis of volcanics and sheeted dikes from the Hatay (Kizildag) Ophiolite, southern Turkey; possible formation with the Troodos Ophiolite, Cyprus, along fore-arc spreading centers. Tectonophysics 223 (3–4), 237–272.

Lytwyn, J.N., Casey, J.F., 1995. The geochemistry of postkinematic mafic dike swarms and subophiolitic metabasites, Pozanti–Karsanti ophiolite, Turkey: evidence for ridge subduction. GSA Bulletin 107 (7), 830–850.

Mahmood, K., Boudier, F., Gnos, E., Monie', E.P., Nicolas, A., 1995. $^{40}Ar/^{39}Ar$ dating of the emplacement of the Muslim Bagh ophiolite, Pakistan. Tectonophysics 250, 169–181.

Moores, E.M., 1982. Origin and emplacement of ophiolites. Rev. Geophys. Space Phys. 20, 735–760.

Munir, M., Ahmad, A.Z., 1985. Petrochemistry of the contact rocks from northwestern Jang Tor Ghar segment of the Zhob Valley ophiolite, Pakistan. Acta Mineral. Pak. 1, 38–48.

Nakagawa, M., Siddiqui, R., Hoshino, K., 1996. Chemical compositions of chromites from the Saplai Tor Ghar Massif of the Muslim Bagh Ophiolites, western Pakistan. In: Yajima, J., Sifddiqui, R.H. (Eds.), Proceedings of Geoscience Colloquim, 16. Geoscience Laboratory, Geological Survey of Pakistan, Islamabad, pp. 177–194.

Nicolas, A., Reuber, I., Benn, K., 1988. A new magma chamber model based on structural studies in the Oman Ophiolite. Tectonophysics 151, 87–105.

Ninomiya, Y., 2003. A stabilized vegetation index and several mineralogic indices defined for ASTER VNIR and SWIR data. IEEE International Geoscience and Remote Sensing Symposium: Proceedings: Centre de Congre's Pierre Baudis, Toulouse, France, pp. 1552–1554.

Ninomiya, Y., Fu, B., Cudahy, T.J., 2005. Detecting lithology with Advanced Spaceborne Thermal Emission and Reflection Radiometer (ASTER) multispectral thermal infrared “radiance-at-sensor data. Remote Sens. Environ. 99, 127–139.

Otsuki, K., Hoshino, K., Anwar, M., Mengal, J.M., Broahi, I.A., Fatmi, A.N., Yuji, O., 1989. Breakup of Gondwanaland and emplacement of ophiolitic complexes in Muslim Bagh area of Balochistan, Pakistan. In: Okimura, Y., Fatmi, A.N. (Eds.), Tectonics and Sedimentation of the Indo-Eurasian Colliding Plate Boundary Region and Its Influence on the Mineral Developments in Pakistan. Hiroshima Univ., pp. 33–57.

Parlak, O., Delaloye, M., 1999. Precise $^{40}Ar/^{39}Ar$ ages from the metamorphic sole of the Mersin ophiolite (Southern Turkey). Tectonophysics 301, 145–158.

Parlak, O., Hock, V., Delaloue, M., 2002. The supra-subduction zone Pozanti–Karsanti ophiolite, southern Turkey: evidence for high-pressure crystal fractionation of ultramafic cumulates. Lithos 65 (1–2), 205–224.

Parlak, O., Delaloye, M., Bingol, E., 1996. Mineral chemistry of the arc-related ultramafic–mafic cumulates as an indicator of the arc-related origin of the Mersin ophiolite (southern Turkey). Geol. Rundsch. 85 (4), 647–661.

Pearce, J.A., 2003. Supra-subduction zone ophiolites: the search for modern analogues. In: Dilek, Y., Newcomb, S. (Eds.), Ophiolite Concept and the Evolution of Geological Thought. GSA spec. publ, 373, pp. 269–294.

Polat, A., Casey, J.F., Kerrich, R., 1996. Geochemical characteristics of accreted material beneath the Pozanti–Karsanti Ophiolite, Turkey; intra-oceanic detachment, assembly and obduction. Tectonophysics 263 (1–4), 249–276.

Robertson, A.H.F., 2002. Overview of the genesis and emplacement of Mesozoic ophiolites in the Eastern Mediterranean Tethyan region. Lithos 65, 1–67.

Rossman, D.L., Ahmad, Z., Rehman, H., 1971. Geology and economic potential for chromite in the Zhob Valley Ultramafic Complex (Jang Tor Ghar) Hindubagh, Quetta Division, West Pakistan. Geol. Survey and U.S. Geol. Survey Interim Report.

Rothery, D.A., 1987. The role of Landsat multispectral scanner (MSS) imagery in mapping the Oman Ophiolite. J. Geol. Soc. London 144, 587–597.

Rowan, L.C., Mars, J.C., Simpson, C.J., 2005. Lithologic mapping of the Mordor, NT, Australia ultramafic complex by using the Advanced Spaceborne Thermal Emission and Reflection Radiometer (ASTER). Remote Sens. Environ. 99, 105–116.

Searle, M.P., 1986. Structural evolution and sequence of thrusting in the High Himalayan, Tibetan Tethys and Indus Suture zones of Zannsker and Ladakh, western Himalaya. J. Struct. Geol. 8, 923–936.

Sillitoe, R.H., 1978. Metallogenic evolution of a collisional mountain belt in Pakistan: a preliminary analysis. J. Geol. Soc. London 135, 377–387.

Shervais, J.W., 2003. Birth, death, and resurrection; the life cycle of suprasubduction zone ophiolites. Geochem. Geophys. Geosystem - G 3 2 (1), 1525–2027.

Stern, R.J., Bloomer, S.H., 1992. Subduction zone infancy; examples from the Eocene Izu–Bonin–Mariana and Jurassic California arcs. Geol. Soc. Am. Bull. 104, 1621–1636.

Sultan, M., Arvidson, R.E., Sturchio, N.C., Guinness, E.A., 1987. Lithologic mapping in arid regions with Landsat thematic mapper data: Meatiq dome, Egypt. Geol. Soc. Am. Bull. 99, 748–762.

Tapponnier, P.M., Mattauer, F.P., Cassaigneau, C., 1981. Mesozoic ophiolite, sutures, and large scale tectonic movements in Afghanistan. Earth Planet. Sci. Lett. 52, 355–371.

Treloar, P.J., Izatt, C.N., 1993. Tectonics of the Himalayan collision between the Indian Plate and the Afghan Block: a synthesis. In: Treloar, P.J., P.J., M.P., Searle (Eds.), Himalayan Tectonics. Geol. Soc. Lond. Spec. Publ., vol. 74, pp. 69–87.

Utke, A., Siad, A., 1993. Geomathematical optimization of Landsat-TM satellite data for geological mapping in an island arc/ophiolite environment of the Red Sea Hills, Sudan. In: Thrweihe, Schandelmeier (Eds.), Geoscientific research in Northeast Africa; Proceedings of the International Conference, pp. 117–120.

Van der Meer, F.D., Vazquez-Torres, M., van Dijk, P.M., 1997. Special characterization of ophiolite lithologies in the Troodos ophiolite complex of Cyprus and its potential in prospecting for massive sulphide deposits. Int. J. Remote Sens. 18 (6), 1245–1257.

Yalınız, M.K., Göncüoğlu, M.C., Özkan-Altıner, S., 2000. Formation of emplacement ages of the SSZ type Neotethyan Ophiolites in Central Anatolian, Turkey: paleotectonic implications. Geol. J. 35, 53–68.

Yin, A., 2006. Cenozoic tectonic evolution of the Himalayan orogen as constrained by along strike variation of structural geometry, exhumation history, and foreland sedimentation. Earth-Sci. Rev. 76, 1–131.